

Best of two worlds: Cartesian sampling and volume computation for distance-constrained configuration spaces using Cayley coordinates

Yichi Zhang¹ and Meera Sitharam¹
Department of CISE, University of Florida ^{a)}

(*Electronic mail: sitharam@ufl.edu)

(Dated: 2 September 2024)

Volume calculation of configurational spaces acts as a vital part in configurational entropy calculation, which contributes towards calculating free energy landscape for molecular systems. This task is typically handled by sampling and counting in configurational space using mapping between two coordinate systems: an "internal" coordinate and standard Cartesian. Methods based on this approach share various shortcomings, including computational error and ill-conditioning in matrix derivative (Jacobian and Hessian) used to calculate mapping function, and the so-called "curse of dimensionality" which makes sampling impractical when the input system is large and complex. In this article, we present our sampling-based volume computation method using distance-based Cayley coordinate, mitigating aforementioned drawbacks: our method guarantees that the sampling procedure stays in lower-dimensional coordinate space (instead of higher-dimensional Cartesian space) throughout the whole process; and our mapping function, utilizing Cayley parameterization, can be applied in both directions with low computational cost. Our method uniformly samples and computes a discrete volume measure of a Cartesian configuration space of point sets satisfying systems of distance inequality constraints. The systems belong to a large natural class whose feasible configuration spaces are effectively lower dimensional subsets of high dimensional ambient space. Their topological complexity makes discrete volume computation challenging, yet necessary in several application scenarios including free energy calculation in soft matter assembly modeling. The algorithm runs in linear time and empirically sub-linear space in the number of grid hypercubes (used to define the discrete volume measure) *that intersect* the configuration space. In other words, the number of wasted grid cube visits is insignificant compared to prevailing methods typically based on gradient descent. Specifically, the traversal stays within the feasible configuration space by viewing it as a branched covering, using a recent theory of Cayley or distance coordinates to convexify the base space, and by employing a space-efficient, frontier hypercube traversal data structure. A software implementation and comparison with existing methods is provided.

I. INTRODUCTION

A. Attempts of Volume Calculation

Access to accurate free energy landscape is key for multiple kinds of approaches in researching molecule-level processes. As a vital part of energy calculation, the calculation of entropy in molecular systems remains important since Boltzmann formulated calculation of entropy in the 1870s. Specifically, for free energy landscape with multiple basins, relative ratio of basin volume directly corresponds to relative entropy level between them.¹

Methods based on classical statistical mechanics are thoroughly researched on simple models of physical systems, such as hard disks², hard spheres³, and dumbbells (as modeling for diatomic molecules)⁴. Such method can also be applied on more complex systems.⁵ tabulated configurational entropy of more than 100k small molecules using statistical mechanics model with corrections from experimental data.

Entropy of more complex systems, such as macromolecules (for instance, proteins) in biology, remains a research topic highly of interest for more than 40 years.⁶⁻⁹. Multiple methods have been tested and applied for different processes involving proteins, including folding^{10,11}, recognition¹² and

docking^{13,14} of small molecules, binding between protein-protein¹⁵⁻¹⁷ and protein-ligand¹⁸⁻²¹, etc.

Computational chemists have been trying to tackle the problem of calculating conformational entropy with volume of configurational space for decades with widely used computational molecular science approaches, such as Monte Carlo algorithm and Molecular Dynamics²². Methods based on Monte Carlo^{10,23} are affected by the curse of dimensionality: when the system grows larger, these methods would perform random-walk in very high dimensional configurational space, showing their general inability to reduce the dimensionality, making calculation impractical especially when number of objects in system is large.

Molecular Dynamics methods attempt to reduce the dimensionality by converting between two coordinate systems, namely Cartesian and internal coordinates²⁴, and use matrix derivatives - such as Jacobian and Hessian - of the mapping function to calculate steps for traversing the entire configurational space²⁵. Different methods of choosing internal coordinates are applied, including natural internal coordinate^{26,27}, redundant internal coordinate^{28,29}, delocalized internal coordinate^{30,31} etc. All these methods fall short for requiring computationally expensive pseudo inverses such as the Moore-Penrose which leads towards both high time cost and potential errors. More recently,³² reported using higher order derivatives and their Taylor expansion to calculate steps for the sampling procedure and performed more efficient and reliable than traditional methods, and³³ focused on a coordinate system specified towards molecular vibrations. Soft-

^{a)}M.S. affiliated with Department of Mathematics.

ware level optimization on the transformation between Cartesian and internal coordinates is also performed^{34,35}, including involving machine learning-based predictions³⁶. However, problems that arise from the nature of these methods still remain. Namely, linearization in numerical calculation creates error, and it will in turn harm the quality of the traversal of configurational space; also, ill-conditioning of the mapping function for some region of the configurational space will also greatly hinder the viability of using such methods for volume calculation, and entropy as well³⁷.

In this article, we present a novel way using **EASAL**, our state-of-the-art molecule sampling tool based on Cayley parameters, to calculate configurational entropy in molecular systems. EASAL samples lower dimensional regions of the entire conformational space (instead of the entire one) so the curse of dimensionality can be mitigated. For discrete volume calculation, we take advantage of EASAL’s Cayley parameterization and use that as our version of "internal coordinate"; then, we designed **Uniform Cartesian** algorithm to utilize the specialty of our 2 coordinate systems (Cayley and Cartesian) so that direct calculation of derivatives of the mapping function can be replaced with a procedure of mapping and intersection checking performed in Cayley space; linearization error is also mitigated by applying specifically designed way of decomposing hypercubes in Cartesian space and mapping to Cayley.

A common type of configuration space is a feasible region of a distance constraint system between *point sets*, i.e., consisting of configurations of a finite collection of (internally rigid) point sets in \mathbb{R}^d that satisfy a distance constraint system (equalities and/or inequalities) between points in different point sets. Each of the point set is an equivalence class of point sets modulo a group of isometries, which, in the case of Euclidean distance constraint systems, typically consists of rotations and translations. Examples of such configuration spaces occur in the study of kinematic mechanisms, (under-constrained) mechanical CAD designs, molecular or particle assemblies, metamaterials, etc.

B. Contributions and Significance

In the above-mentioned scenarios, uniformly sampling and computing (relative) discrete volume measures of effectively lower dimensional and topologically complex spaces of higher dimensional ambient spaces are crucial tasks in several application scenarios. Examples include free energy and configurational entropy computation³⁸ for relatively simple systems of soft-matter assembly driven by (short-ranged) Lennard-Jones potentials that continue to challenge prevailing molecular dynamics or Monte Carlo based methods^{31,32,36,39,40}.

(1) The first contribution is an efficient algorithm *Uniform Cartesian* that uniformly samples (and thereby computes a discrete volume measure) of a large, well-defined and commonly occurring class of distance constrained configuration spaces with desired accuracy in linear output complexity. In addition to leveraging a previous sampling method (*) de-

scribed in ID that treats the configuration space as a branched covering space of a convex base space represented in Cayley coordinates^{41,42}, our algorithm is inspired by a slicing algorithm for 3D printing very large objects filled with mapped (curved) microstructures⁴³. See Figures 1 C, 2 and 3.

(2) The second contribution is of independent interest: a space-efficient traversal method for grid hypercubes of the ambient space that intersect the effectively lower dimensional configuration space. The method empirically (and intuitively) takes sublinear space in the number of such grid hypercubes.

(3) The third contribution is an opensource software implementation of the above algorithm that is used to compare the performance of our method using 3 variants of the previous method (*) of^{41,42}. These variants were already shown to have specific performance advantages in comparison to prevailing Monte Carlo based methods in⁴⁴.

C. Preliminaries and Background

A typical *distance constraint system* is specified by a finite set S of point sets together with a constraint graph G each of whose vertices v is a point on the point set $S(v)$ and whose edges represent distance (interval) constraints. The variables are the *Cartesian* orientations T_X for $X \in S$, given by $\binom{d+1}{2}$ scalars specifying X ’s rotation and translation relative to some fixed $O \in S$, where T_O is assumed to be the identity. The entire constraint system (C) is specified as follows:

- (C1) For every pair (A, B) in S and every pair of points $a \in A$ and $b \in B$, $\|T_A(a) - T_B(b)\| \geq l(a, b)$,
- (C2) For every edge $(a, b) \in G$, $l(a, b) \leq \|T_{S(a)}(a) - T_{S(b)}(b)\| \leq h(a, b)$

Here h and l are given positive scalar functions. For the problems considered in this paper, we will assume – essentially without loss of generality – that (i) the limiting case where the interval size $h(a, b) - l(a, b)$ tends to 0 as this case is both more difficult and more interesting; and (ii) that G is independent and flexible in the sense of combinatorial rigidity^{45,46}. Furthermore, while this paper deals only with Euclidean distance constraints, the concepts generalize to non-Euclidean norm or even other metric distance constraints.

Typically, such Cartesian configuration spaces are topologically complex semi-algebraic subsets of a high dimensional ambient space (k point sets give $m = (k-1)\binom{d+1}{2}$ ambient dimensions). Generically, when the constraints as in (C2) above satisfy $l = h$, the configuration space is a real algebraic (quadratic) variety of co-dimension $|E(G)|$. However, in the abovementioned applications, typically, the distance constraints are either unidirectional inequalities, or, if they are bidirectional then the specified intervals of allowable distances are typically "small" as indicated in the assumption above.

A common example is a discretized version of a so-called Lennard-Jones potential constraint between 2 atoms in assembling rigid molecules⁴⁷. Such potentials encode a variety of

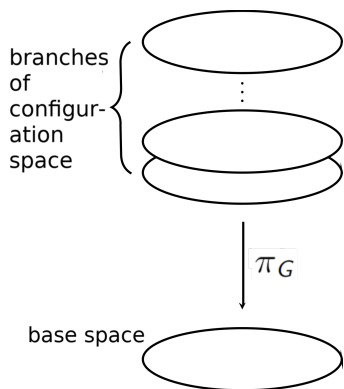


FIG. 1. Schematic illustration of continuous covering map, finitely many branches or flips of preimage branched covering space, and base space.

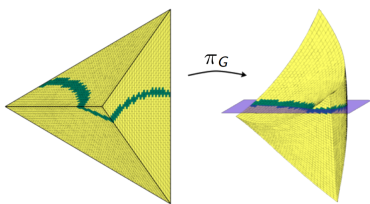


FIG. 2. schematic of a 2-dimensional feasible configuration space R (green) in 3-dimensional ambient space (yellow), intersecting grid cubes, before and after map π_G is applied (figure courtesy⁴³). The ambient space is 6-dimensional in this paper.

types of weak interactions, including Van der Waals, hydrogen bonds, as well as electrostatic, hydrophobic, hydrophilic, and quantum-level interactions.

Each such interval constraint effectively reduces the dimension of the configuration space by one so that we are dealing with a configuration space that is effectively of much smaller dimension than the ambient dimension. For example $m - 1$ (resp. $m - 2$) such “small” interval constraints would generically yield a configuration space that is a “thick” curve (resp. sheet) in the ambient m dimensional space, with the thickness tending to 0 in the limiting case. See examples in fig 3.

Whether dealing with distance equality or inequality constraints, the task of traversing or sampling configurations while staying within the effectively lower dimensional and topologically complex Cartesian configuration space is typically achieved using an onerous type of “gradient descent”, i.e. repeated linear tangential steps (e.g. by computing the Jacobian of the distance map of the constraint system), alternating with projections / corrections back to the feasible region. When prevailing methods are used, including molecular dynamics or Monte Carlo based methods, this gradient descent process pervades many common tasks such as finding optimal or extremal configurations, finding paths, path lengths, region volumes (configurational entropy), path probabilities for transition networks, sampling configurations or paths etc.

D. Previous Work

The papers^{41,42,48–52} solved the problem of traversing or sampling – while staying within – a distance constrained, Cartesian configuration space, by treating it as a *branched covering space*.

More precisely, a configuration space in m ambient dimensions, defined as in (C2) above by a constraint graph G of $|E(G)|$ generically independent distance (interval) constraints, is mapped by a *covering map* to a *base space* that is a subset of the space spanned by $m - |E|$ Cayley coordinates (see fig 1C). A *Cayley coordinate* is an unconstrained pairwise squared distance associated with a nonedge in the distance constraint graph. A *Cayley configuration* is a tuple of $m - |E|$ Cayley coordinate values; the base space consists of Cayley configurations. By definition of a covering map, the pre-image of a Cayley configuration is finite, i.e. has generically at most finitely many feasible configurations mapped to it by the covering map. Accordingly, the pre-image of the base space is the union of finitely many almost disjoint “sheets” or *flips*, which are branches of the covering space. The flips or branches may intersect on a set of dimension strictly smaller than $m - |E|$. See fig 3.

For dimension $d \leq 3$ and a substantial *nice* class \mathcal{C}_d of distance (interval) constraint graphs G ,^{41,42,48} used the properties of the cone of Euclidean squared pairwise distances of a point set⁵³ (which can be generalized to other norms⁵⁴) to show the following properties: (1) there is a covering map π_G given by chosen Cayley coordinates or non-edges of G , guaranteeing a convex base space (consisting of feasible Cayley configurations with nonempty pre-images of the covering map); (2) for a Cayley configuration in the base space, computing the pre-image configurations of the covering map has linear output complexity; and (3) determining whether a Cayley configuration is feasible has linear time complexity in the problem size i.e. the number of points specifying the point sets. We note that the original paper⁴⁸ states these properties for a larger graph whose edges - interpreted in the context of this paper - include the distance constraints between point pairs within each point set. However the the graph G in papers^{41,42} refers only to the distance (interval) constraints (C2) between point sets.

Using these properties, one can efficiently traverse the effectively lower dimensional and topologically complex feasible configuration space R as follows. Traversing the base space of R is efficient by (1) and (3) above, and moreover a subset of the Cayley coordinate space, by definition; computing the pre-image configurations of the covering map is efficient by (2) above. This yields a traversal that does not leave the branched covering space R . Furthermore, the *boundaries* of the base space of R are explicitly detected and traversed. The boundaries represent two types of transitions: (i) the inequalities in (C1) and (C2) above become tight, or (ii) the real pre-image of the covering map becomes empty (the pre-image is complex); these are additionally the intersections of the branches or flips of the covering space.

The Cayley configuration methodology requires characterizing distance constraint graphs with convex base spaces of

Cayley configurations. It draws upon a rich set of tools from graph rigidity, realization and distance geometry^{45,46}, generalizes to other norms⁵⁵ is closely related to a key finite forbidden minor property called flattenability of graphs⁵⁵⁻⁵⁷, and leads to directions of independent interest to those areas. Furthermore, the methodology has been implemented as open-source software (EASAL^{41,42} and CayMos^{49,50}) for respectively molecular and particle assembly modeling and kinematic mechanism analysis and design) and has led to several improvements in those areas, besides efficient algorithms for the core problem of distance constraint graph realization⁵⁸.

II. PROBLEMS, OBSTACLES AND DETAILS OF CONTRIBUTIONS

While the Cayley coordinate representation significantly improves the efficiency of traversal, path finding, search for extremal configurations, etc.^{41,42,44,49-52}, for a configuration space specified by distance constraint graphs in the abovementioned class \mathcal{C}_d of⁴⁸, it is not clear how to use it to sample the configuration space uniformly in the original *Cartesian* coordinates of the ambient space, or to compute volume measures (or path lengths), a frequent and important task for configurational entropy and free energy computations^{11,59,60}. Such volume definitions are based on a Cartesian coordinate grid.

Problem 1 is to compute the ε -approximate *volume* of a (feasible) configuration space R in ambient m -dimensional Cartesian coordinate space, defined as the relative proportion of m -dimensional hypercubes of side length ε that intersect R (in a generic rectilinear grid subdivision of the ambient space).

Problem 2 is to generate one point on R per intersecting hypercube, i.e. a uniform Cartesian sampling of configurations in R . Both problems assume distance constraint graphs in the nice class \mathcal{C}_d .

Clearly Problem 1 reduces to Problem 2 but it is conceivable that it could be solved directly. As we explain the approaches to Problem 2 below, we note the reasons why, in current practice, Problem 1 is solved essentially by solving Problem 2.

One obvious way (*) to try to solve both problems is to use the known efficient method^{41,42,49,50} for uniform sampling in Cayley coordinates of R 's convex base space together with preimage computations as described above, since R 's distance constraint graph is in the nice class \mathcal{C}_d . However, with no adjustments, this results in a highly nonuniform sampling of R , i.e. an unsatisfactory solution to Problem 2, see fig 3.

In fact, this is a decades-old problem in computational chemistry, referred to as "internal coordinate to Cartesian back transformation", that continues to be actively studied^{31,32,36}. To clarify, the "internal coordinates" used in computational chemistry, e.g. in molecular dynamics, are different from Cayley coordinates, and to the best of our knowledge lack the underlying theory and tools available for Cayley coordinates.

The straightforward workaround is to traverse the base space of R in Cayley coordinates, but iteratively adjust the size of each Cayley step by computing a pseudoinverse of the linearization (Jacobian) of the covering map and ensuring

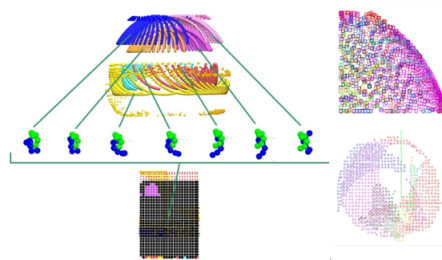


FIG. 3. Screenshots obtained using the opensource software EASAL: **Left:** Top: Two dimensional Cartesian configuration space R (of a distance constraint system in dimension 3) in 6-dimensional ambient space, projected on the 3 translational coordinates, non-uniformly sampled; colors represent different flips of R viewed as a branched covering space. Middle: some sampled feasible configurations of point sets satisfying distance constraints of the type (C1) and (C2), one from each flip. Bottom: corresponding convex base space with uniform sampling in Cayley coordinates.

Right: Bottom: Uniform Cartesian sampling, colors represent different flips of another two dimensional configuration space R (also in 6-dimensional ambient space projected on 3 translational coordinates, also of a distance constraint system in dimension 3 not shown) as a branched covering space. Top: Corresponding (nonuniform) sampling of the convex base space in Cayley coordinates, note that some Cayley configurations have multiple colors - each such configuration has finitely many preimages each belonging to a different flip. (figure courtesy of⁶¹).

uniform Cartesian sampling of the pre-image branched covering space R . This approach suffered from both inaccuracies due to linearization error as well as illconditioning problems, thus had overall unreliable performance on accuracy and efficiency⁶¹. A standard way to address these problems is to use the Hessian and higher derivatives of the covering map. However, such efforts are still underway^{31,32,36} and the problem is by no means settled. It should be noted that the use of higher derivatives of the covering map theoretically provides another approach to Problem 1 directly without Problem 2. I.e., one could avoid uniform Cartesian sampling of the configuration space R , but rather use the convexity advantage of the base space to compute its Cayley volume in polynomial time using a random walk⁶²⁻⁶⁶, while using the higher derivatives of the covering map to compute the volume of R and solve Problem 1. In any case, this too involves some form of randomized or deterministic adaptive sampling in Cayley coordinates. Furthermore, to our knowledge such an approach to Problem 1 that avoids Problem 2 does not exist in the literature. One reason could be that although the covering map is quite well behaved, this cannot be said about the pseudoinverses of its Jacobian or Hessian. Our contributions provide an optimal solution to Problem 2 and thereby a solution to Problem 1.

A. Details of Contributions

(1) The first contribution is an algorithm *Uniform Cartesian* that solves Problem 2 when the graph G is in the above-

mentioned class \mathcal{C}_d for $d \leq 3$ (as characterized in^{42,48}) in time linear in the output size, i.e. in the number of ε -cubes that intersect R . This is optimal (and nontrivial) since R is a topologically complex, effectively lower dimensional subset of the ambient space. In addition to leveraging the known efficient method (*) for sampling the base space of R in Cayley coordinates^{41,42}, our algorithm is inspired by a slicing algorithm for 3D printing very large objects filled with mapped (curved) microstructures⁴³. See Figures 1C, 2 and 3.

(2) The second contribution is of independent interest: a space-efficient grid traversal method that empirically (and intuitively) takes sublinear space in the number of grid cubes visited. This indicates sublinear space complexity (in terms of output size) for a modified Problems 1 and 2 that requires *at least* (instead of exactly) one point per grid hypercube that intersects R .

(3) The third contribution is an opensource software implementation of the above algorithm that is used to compare the performance of our method for Problem 1 using variants of the obvious method (*) described above, i.e., Cayley sampling according to 3 different distributions together with pre-image computations of the covering map. These variants were already shown to have significant advantages in efficiency and efficiency-accuracy tradeoffs, in comparison to prevailing Monte Carlo based methods in⁴⁴. The implementation relies on efficient grid hypercube representations that could be of independent interest: they speed up the extraction of arbitrary dimensional facets and simplices and their intersection with the configuration space R .

III. CONTRIBUTIONS 1 AND 2: SAMPLING ALGORITHM AND INTERSECTING HYPERCUBE TRAVERSAL DATA STRUCTURE

Input: a set of point sets S , and constraints as in (C) with the constraint graph G in the class \mathcal{C}_d , $d \leq 3$ together with bounds l and h . These define the configuration space R . The required accuracy ε for Problems 1 and 2. For reasons of exposition and the current software implementation, we further assume $d = 3$ and $|S| = 2$ whereby the ambient dimension $m = 6$. Smaller d are subsumed. Larger d lack characterization of the “nice” class \mathcal{C}_d . For larger S , the current contribution goes through for constraint graphs G in \mathcal{C}_d . However, for larger S , many constraint graphs fall outside the \mathcal{C}_d and have to be dealt with. For this problem (separate from the current one), an algorithm for $|S| > 2$ is covered in⁴². We further assume the modified Problems 1 and 2 that require *at least* (instead of exactly) one point per grid hypercube that intersects R . A straightforward output data structure with a hash map solves the original problems efficiently.

The algorithm has 4 parts.

1. using the covering map π_G given in⁴⁸, to **sample the base space** $\pi_G(R)$ in Cayley coordinates using the method in⁴² that determines a Cayley step-size based on ε and finds boundaries and extremal configurations; further compute the corresponding pre-image Cartesian

configurations s in R . Then, split s into portions corresponding to each flip.

2. For each flip f , using the Cartesian ε -grid hypercube containing s_f as a starting point, **generate hypercubes p on-demand, and traverse using a key frontier hypercube data structure.**
3. Use the covering map π_G to generate Cayley cuboid $\pi_G(p)$, then **calculate the intersection with region $\pi_G(R_2)$ of dimension $m - |E(G)|$** ; here R_2 is the set of configurations satisfying the constraints (C2) and $R \subseteq R_2$; this generates partly feasible Cayley configurations c .
4. Compute the pre-image configurations $\pi_{G,f}^{-1}(c)$, retain only if fully feasible, i.e. only if (C1) is satisfied, and **find and count the corresponding Cartesian grid cube p'** if p' is in flip f . Note that due to linearization error, p may differ from p' . This solves the modified Problems 1 and 2. A straightforward output data structure stores the cubes p' and locates them with a hash map to avoid double counting. This solves the original unmodified problems.

We further describe steps 2 and 3 in detail in the following paragraphs.

A. Intersection Calculation of Step 3

Step 3 in the overall algorithm is challenging due to the following reasons:

- π_G is a nonlinear (quadratic) map, thus $\pi_G(p)$, the mapped cuboid in base space, is a complicated nonlinear object, making direct intersection calculation unrealistic;
- Intersecting $\pi_G(p)$ and $\pi_G(R_2)$ yields a potentially disconnected $(m - |E(G)|)$ -dimensional region without a tractable description.

To tackle both issues, we provide a series of workaround operations to calculate intersection:

1. Instead of using a single, m -dimensional $\pi_G(p)$ in intersection calculation, decompose p into a collection of $|E(G)|$ -dimensional objects $\{p_1, p_2, \dots\}$ and map each p_i to $\pi_G(p)_i$ in Cayley space.
2. Define approximation function $L(\cdot)$ based on linearization, apply it to each $\pi_G(p)_i$ to get $L(\pi_G(p)_i)$, which is also $|E(G)|$ -dimensional.
3. Calculate intersection between $L(\pi_G(p)_i)$ and $\pi_G(R_2)$ by solving a system of $|E(G)|$ linear equations for a convex combination.

Taking advantage of co-dimension between $L(\pi_G(p)_i)$ ($|E(G)|$ -dimensional) and $\pi_G(R_2)$ ($(m - |E(G)|)$ -dimensional), intersections obtained are generally 0-dimensional, i.e. points. And after such operations, each p_i

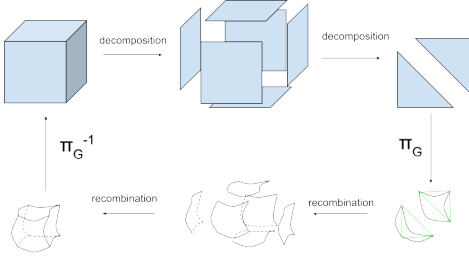


FIG. 4. Schematic illustrating decomposition of a Cartesian hypercube into appropriate dimensional simplices, and linearized simplices of corresponding Cayley cuboid.

can generate at most one intersection point c_i due to linearity of both $L(\pi_G(p)_i)$ and $\pi_G(R_2)$. Set of all intersection points generated this way is then sent into Step 4 of the overall algorithm as input.

We hereby provide 3 different ways of mapping, decomposing, and linearizing p into set of $L(\pi_G(P)_i)$, alongside one extra attempt for a more specific case that matches experimental results we are comparing our method against.

1. Decomposition based on simplicial element - regular-UC

$\pi_G(\cdot)$ maps a Cartesian simplex into a curved simplex in Cayley space. Define linearization $L(\cdot)$ on a curved simplex as rebuilding the simplex with all its vectors, then simplex s will generally hold its dimensionality after the transformation. To decompose hypercube p , following steps are performed:

1. Decompose p into $|E(G)|$ -dimensional facets.
2. Decompose each facet f into $|E(G)|$ -dimensional simplices s .
3. Calculate $\pi_G(V(s))$, i.e. map the set of vertices of s into Cayley.
4. Build Cayley simplex $L(\pi_G(s))$ using $\pi_G(V(s))$ as vertices.

This definition of $L(\pi_G(\cdot))$ on simplices is simple and straightforward while keeping crucial information of simplices. However, we observed significant linearization error especially when p is close to border of R defined by (C1), as well as potential to speed up the process by approximating more aggressively and omitting some of the data. Modifications towards these goals are covered in the following paragraph.

This method is referred to as **regular-UC** in latter part of this article.

2. Modified decomposition on simplicial element - face-UC and hybrid-UC

Coordinates of $(m-1)$ -dimensional face centers are vital in avoiding distortion caused by linearization mentioned in the

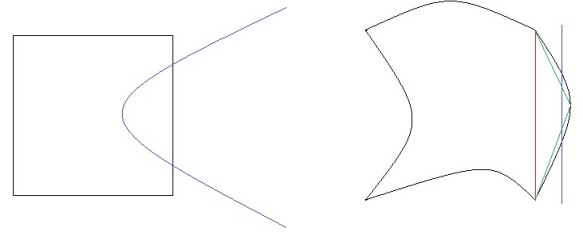


FIG. 5. Illustration in 2-dim for simplicial decomposition error. **Left:** p (black) and R_2 (blue), **Right:** $\pi_G(p)$ (black), $\pi_G(R_2)$ (blue), $L(\pi_G(s))$ using regular(red) and modified(green) linearization. Modified linearization helps finding intersections that are otherwise missed with regular linearization.

previous paragraph, see fig 5. We modify the decomposition procedure as follows:

1. Decompose p into $(m-1)$ -dimensional faces.
2. Decompose each $(m-1)$ -dimensional face F into $(|E(G)-1|)$ -dimensional facets.
3. Decompose each facet f into $(|E(G)-1|)$ -dimensional simplices s .
4. Build $|E(G)|$ -dimensional Cartesian simplex s' with $V(s)$ and center of F , the corresponding $(m-1)$ -dimensional face center.
5. Calculate $\pi_G(V(s'))$.
6. Build Cayley simplex $L(\pi_G(s'))$ using $\pi_G(V(s'))$ as vertices.

This method is referred to as **face-UC**.

The design decision of using $(m-1)$ -dimensional face centers is to avoid significant distortion due to linearization error. During development, we first tried to use m -dimensional cube centers in decomposition procedure, but made the decision to switch to using $(m-1)$ -dimensional centers instead, due to the fact that decomposition involving m -dimensional centers does not capture the distortion on mapping function, especially when it is large enough that the m -dimensional cube center in Cartesian is not in the mapped cube. Illustration can be found in fig 5

This method improves the accuracy at the cost of higher time consumption. To lower overall resource cost, we opt to combine aforementioned 2 methods to speed up the procedure. Firstly, regular decomposition is performed on each hypercube, and when it fails to find any feasible intersection, face center version is used. We name this hybrid approach of regular- and face-UC as **hybrid-UC**, and it is used as our main tool in calculating volumes.

3. Decomposition based on hyper-parallelepiped element - basis-UC

We would also like to have a relatively coarse, yet fast variant of our algorithm. To achieve this, we introduce the follow-

ing method.

Instead of simplices, stop decomposition at facet level. Define $L(f)$ for Cartesian facet as hyper-parallelepiped centered at $\pi_G(f.center)$ and spanned by a set of basis vectors calculated from p . Such approach retains the property of easy intersection calculation with co-dimensional Cayley region. This method reduces the total number of linear combination calculations to a fraction of previous methods', due to the fact that each facet (instead of simplex) will generate at most 1 intersection.

1. From p , get all $(m - 1)$ -dimensional face centers F .
2. Map $F.center$ into Cayley space as $\pi_G(F.center)$ and calculate set of basis vectors using $\pi_G(F.center_i)$ of opposing faces.
3. Decompose p into $|E(G)|$ -dimensional facets f .
4. Span hyper-parallelepiped $\pi_G(f)$ in Cayley space with $\pi_G(f.center)$ as center and corresponding basis vectors from step 2.

We name this method **basis-UC** as it uses basis vector of hyper-parallelepiped to calculate intersection.

4. *Special case towards loosening (C2):* $|E(G)| = 1$ - **thick-UC**

Cases mentioned above all regard (C2) as a group of **equations**. When we loosen such constraints to be ranges (as our users potentially desire), changes have to be made to sample this new "thick" R as intersection calculation becomes harder as R becomes m -dimensional. However, with (C2) being range constraints, EASAL provides method to check whether a Cayley point v meets such range constraints. To calculate whether a cube p intersects $\pi_G(R_2)$, we map it into a Cayley point set and check if any of the points in the set is within range determined by (C2). Here we discuss one specific case when $|E(G)| = 1$, i.e. (C2) consists of only 1 range constraint, referred to as 5-dim **thick-UC** in latter part of this article.

1. Decompose p into 1-dimensional segments s following modified decomposition method.
2. For each s , map both vertices into Cayley. $L(\pi_G(s))$ is a segment in Cayley space.
3. Equally divide $L(\pi_G(s))$, get set of dividing points v .
4. Check each v against (C2).

It is worth noting that expanding the usage of this method to cases where $|E(G)| > 1$ is relatively hard, since $L(\pi_G(\cdot))$ is hard to define and point count of all v grows exponentially. Therefore, only $|E(G)| = 1$ version is implemented in the software covered in this paper.

B. The Frontier Hypercube Graph Data Structure of Step 2

Define a hypercube as *inspected* when one of its $(m - 1)$ -dimensional face neighbors is processed in Step 3. Step 2 above is achieved by differentiating between inspected and processed hypercubes and storing only inspected but unprocessed frontier hypercubes in the traversal procedure and discarding interior hypercubes i.e., processed hypercubes whose neighbors have already been inspected. Two inspected hypercube containers, P and Q , are maintained during procedure, with P for *promising* hypercubes yet to be processed, and Q for *not-yet-promising*. A hypercube is deemed promising if one of its face neighbors has a $|E(G)| \leq m$ dimensional facet containing a valid intersection and pre-image in R in their shared $(m - 1)$ dimensional face, and not-yet-promising if some of its face neighbors have been processed but the hypercube is not in P . Each face of a hypercube is given 1 of 3 labels: shared with a processed cube, shared with an unprocessed (and thus unprocessed) cube, or shared with inspected but unprocessed cube. P and Q are implemented as a combination of stack and unordered set (hash map) with relative Cartesian coordinates of a hypercube's center as key and a set of labels, one for each face neighbor, as value.

1. Initialize P with hypercubes generated in Step 1 and Q empty.
2. Pick cube c to process from P . In particular, only facets belonging to faces shared with unprocessed cubes are processed to avoid repetition.
3. Put c 's neighbors into P or Q , or move them from Q to P , based on the result of processing c . Face labels of these neighbors are updated. Remove c from P .
4. Algorithm ends when P is empty.

To elaborate: it is possible that at the time c is chosen from P to be processed, in fact all of c 's faces were shared with previously processed hypercubes, in which case, there is nothing further to be done and c is removed from the data structure. It is also possible that although some of c 's faces were shared with unprocessed hypercubes in P or Q , or uninspected hypercubes, all of c 's $|E(G)|$ dimensional facets could have already been processed. I.e. there is no Step 3 or 4 to be done at the time c is chosen to be processed. In any case, faces corresponding to c 's uninspected or unprocessed face neighbor hypercubes are processed one face at a time. Effectively any of c 's $|E(G)|$ -dimensional facets not shared with processed cubes are processed. The faces corresponding to c 's unprocessed neighbors in P or Q are processed and these neighbors' shared faces with c are appropriately relabeled. In this process, some hypercubes could move from Q to P . Any of c 's uninspected face neighbors that were previously not in the frontier hypercube data structure are now added to P or Q , appropriately labeling those shared faces. At this point, c is considered processed and is removed from the frontier hypercube data structure. *The key property of this data structure is that a hypercube c can be removed as soon as it is processed without compromising the traversal.* Note that P and

Q could contain disconnected components and even singleton hypercube/vertices (all of whose face neighbors have either been processed or have not been inspected). Furthermore, shared faces between two hypercubes in P could already contain $|E(G)|$ -dimensional facets that have yielded points in R : this is because such facets could additionally belong to faces shared with already processed cubes. However, faces corresponding to edges incident on any hypercube in Q cannot contain such a facet.

C. Complexity

The use of the frontier hypercube data structure as described above ensures that the algorithm inspects *all* the Cartesian hypercubes neighboring those hypercubes that intersect R and starts with an intersection point in R . If R in the above sentence were replaced by R_2 , i.e., without the (C1) constraints, the convexity of the base space $\pi_G^{-1}(R_2)$ would ensure that the algorithm does not miss any Cartesian hypercubes that intersect R_2 and therefore R . Step 1 deals with any discontinuity or other violation of convexity in $\pi_G^{-1}(R)$ arising from the constraints (C1), by including as starting points of the traversal at least one (boundary) hypercube in every component of R (in a minimal decomposition of R into convex regions).

Further, since *only* neighbors of R -intersecting hypercubes are inspected, the number of inspected hypercubes that do *not* intersect R is bounded by a constant ($2d$) factor of the number of intersecting hypercubes.

The above observations complete Contribution 1. As noted in the previous section, a further optimization in the frontier hypercube data structure ensures that inspected hypercubes - which are now in the “interior” of the traversal region - are immediately - and safely - deleted from the frontier data structure, ensuring Contribution 2, empirically verified below.

The next section describes Contribution 3.

IV. CONTRIBUTION 3: COMPUTATIONAL EXPERIMENTS AND COMPARISONS

A. Setup

The software for the new algorithm *UC* (*uniform Cartesian*) was implemented atop existing curated opensource suite EASAL (Efficient Atlasing and Search of Assembly Landscapes), and hence denoted *EASAL-UC*. Software is available at http://bitbucket.org/geoplexity/easal_dev; see also video <https://cise.ufl.edu/~sitharam/EASALvideo.mpeg>, and user guide <https://bitbucket.org/geoplexity/easal/src/master/CompleteUserGuide.pdf>. Although EASAL is suited to full-fledged parallel processing, the experiments presented here are merely for proof-of-concept and were run on a single AMD EPYC 75F3 “Milan” CPU node of a supercomputer system with 40 GB of memory assigned, which EASAL-UC uses less than 1GB throughout the process.

The experiments compare EASAL-UC with comparator methods w.r.t. their performance on Problems 1 and 2 on benchmark Cartesian configuration spaces R defined as follows:

Set S consisting of $|S| = k = 2$ point sets A and B in $d = 3$, both of which have 20 points (see fig 6). Thus the ambient dimension $m = \binom{4}{2} = 6$. Our distance constraint systems (C) (see IC) are defined by first assigning every point p in A and B a “radius” r_p . For all test cases not involving thick-UC, the distance interval lower bound $l(a, b)$ in (C1) and (C2) is specified to be $0.95(r_a + r_b)$, and the distance interval upper bound $h(a, b)$ in (C2) is $1.05(r_a + r_b)$. In thick-UC test cases, bounds are set to $0.75(r_a + r_b)$ and $r_a + r_b + 0.9$ respectively to match input given in⁴⁴.

For the constraints in (C2), we form 4 experiment categories with graphs G containing 1, 2, 3, and 4 edges, and 10 different graphs were chosen from each category, all belonging to the “nice” class \mathcal{C}_3 of^{42,48}, and with the largest relative volume of corresponding configuration space (as given by baseline in next paragraph). These give several different constraint systems (C) and correspondingly different 5, 4, 3, and 2-dimensional feasible configuration spaces R (referred to as “configuration space x ”), with appropriate covering maps and convex base spaces.

For each graph, variants of UC including regular-UC, hybrid-UC, and basis-UC are performed to calculate relative volume of configuration space. Furthermore, thick-UC is applied on 5-dim configurational spaces.

Baseline and Comparator Methods We use uniform grid in the Cartesian space mentioned in⁴⁴ as baseline for both volume calculation and sample coverage. Baseline grid is defined as set of points matching constraints mentioned in experiment setup. For 2-dim spaces, baseline grid provides too few points, so an ultra-fine grid (similar to⁶⁷) is used instead.

We chose Metropolis Monte Carlo and EASAL as comparator methods. EASAL is a state-of-the-art Cayley-based sampling distributions available in the existing EASAL software implementation. One rationale for this choice is that comparisons demonstrating these methods’ performance advantages over Monte Carlo/grid, widely used methods among computational molecular scientists, have already been tabulated in⁴⁴. However, its performance on volume calculation is yet to be tested. Specifically, EASAL perform the straightforward approach (*) described in II.

The Cartesian volume of configuration spaces are performed using variants of EASAL-UC (including hybrid, regular, basis for all dimensionalities, and thick for 5-dim only), EASAL, and MC respectively. ϵ for Problem 1 and 2 also determines Cartesian hypercubes, i.e. translational and rotational step sizes, used in UC. They are set to 1 and $\pi/9$ respectively for 5-dim, 4-dim, and 3-dim experiment group, and 0.5 and $\pi/18$ for 2-dim. EASAL’s step size is set to value such that it provides roughly equal number of sample points with hybrid-UC method.

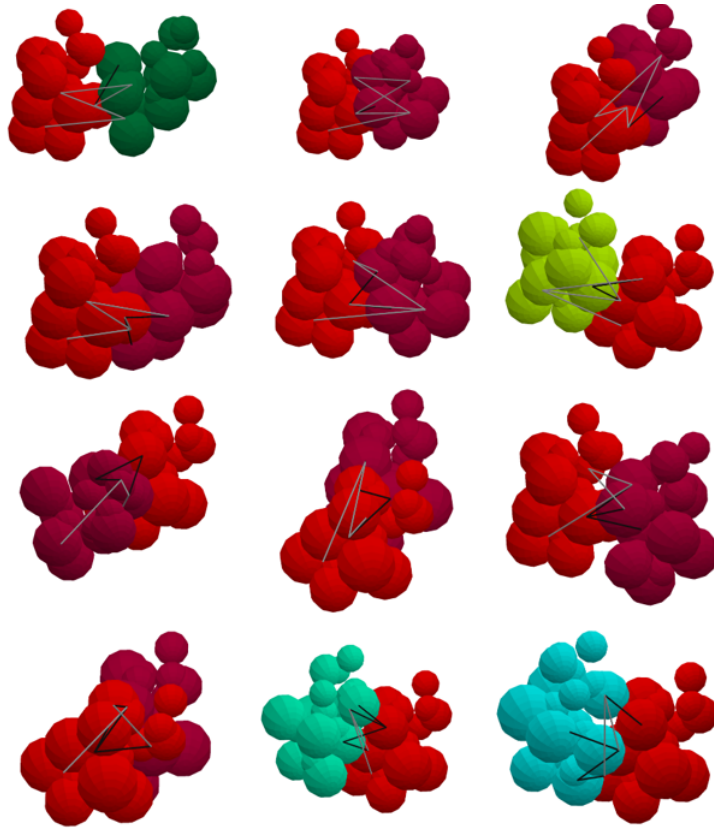


FIG. 6. Input sets S , with different set of constraints (C2) consisting of 1 (1st row), 2 (2nd row), 3 (3rd row), and 4 (4th row) constraints. Spheres of different color represent points belonging to A and B , radii of spheres represent corresponding “radii” of points that specify the distance constraints (C1), black segments between centers of spheres represent constraints in (C2), and grey segments correspond to Cayley parameters chosen. See IC and experimental setup in IV A

B. Key Measurements

We describe the key measurements used to prove our claim on the following topics:

- Is EASAL-UC an improvement over our in-house EASAL implementation, and which variant of EASAL-UC is the best across the board;
- Is the best variant we selected comparable to mainstream methods others are using, such as Monte Carlo.

1. Measurement 1: Volume Calculation Accuracy

UC computes volume of each configuration space by counting Cartesian hypercubes with at least one feasible configuration in them. As for comparator methods, EASAL follows the efficient method (*) mentioned in II, samples the base space in Cayley coordinates according to different distributions, computes the pre-image Cartesian configurations, and counts them to give a rough Cartesian volume approximation; and MC samples by traversing the Cartesian space and volume is calculated alongside traversal using number of samples.

After relative volume of each case is measured, we calculate its ratio against the average of all 10 configuration spaces in the group. Then the result is compared with volume ratio from baseline grid data which is used as a standard.

2. Measurement 2: Efficiency

Number of points sampled by each method is compared across all test case groups. Time cost per sample contributing to volume calculation (i.e. relative volume over total time cost) is also measured for UC and EASAL.

3. Measurement 3: Coverage

Coverage of a method M of baseline Cartesian grid is measured using γ -coverage. A γ -hypercube is a hypercube with a baseline grid point as center and 2γ as range in each Cartesian dimension. A baseline grid point is *covered* by a method M if at least one sample point (center of feasible hypercube for UC) found by M lies with its γ -hypercube. To normalize methods with different number of samples, γ -coverage is defined as the percentage of baseline grid points covered, and

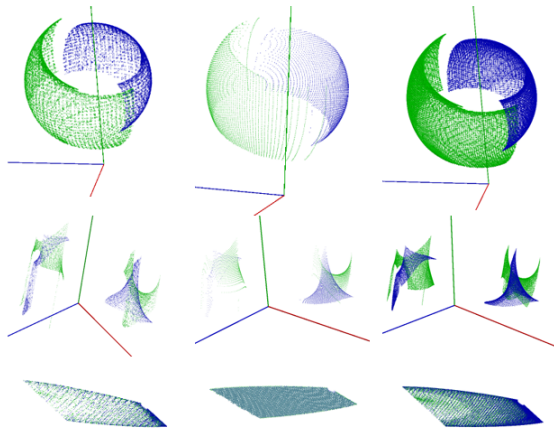


FIG. 7. Performance Screenshots of 2-dimensional configurational regions in 6-dimensional ambient space: Cartesian (Top: projection on 3 translational Cartesian coordinates. Mid: projection on 3 angular Cartesian coordinates) and Bottom: Cayley coordinates of sampled points of the same feasible configuration space/flip. Left: UC, Center: EASAL, Right: Baseline.

the value of γ is set to

$$\gamma := \left(\frac{\Gamma}{\sigma}\right)^{1/6}$$

where Γ is grid point count and σ is sample point count for Method M .

Two aspects of coverage, accuracy and efficiency, are measured in the experiments. Accuracy measurement is done by counting the number of baseline grid points **missing** in the coverage, i.e. no sample point lies within its γ -hypercube. Efficiency of coverage is measured by number of sample points in each γ -hypercube.

4. Measurement 4: Asymmetry Difference between Point Sets

If point sets A and B are identical, then relative volume of systems with 1 constraint $A_i B_j$ and $A_j B_i$ should also be the same. Hence such asymmetry between pairs can be used to determine difference between input point sets. Here we picked 9 corresponding points in A and B , and for the 36 (i, j) pairs, we compare the ratio between volume of $A_i B_j$ and $A_j B_i$. This test works as a follow-up experiment done in⁴⁴.

C. Results

Figure 7 shows screenshots illustrating the relative performance of the EASAL-UC implementation and EASAL against the baseline.



FIG. 8. Volume result for 5, 4, 3, and 2-dim test cases (top to bottom): relative volume among baseline (thick blue), variants of UC (hybrid - red, regular - yellow, basis - green, thick - cyan), and EASAL (orange).

1. Volume Result

Relative volume results are plotted for comparison, with different colors representing different methods (hybrid: red, regular: yellow, basis: green, EASAL: orange, thick: cyan, Monte Carlo: black) and baseline in bold blue line, see fig 8. Better method would have a result closer to baseline. For test cases in each dimensionality, the first plot shows all variants of UC are against original EASAL; then hybrid-UC (and thick-UC for 5-dim test case) is plotted against Monte Carlo,

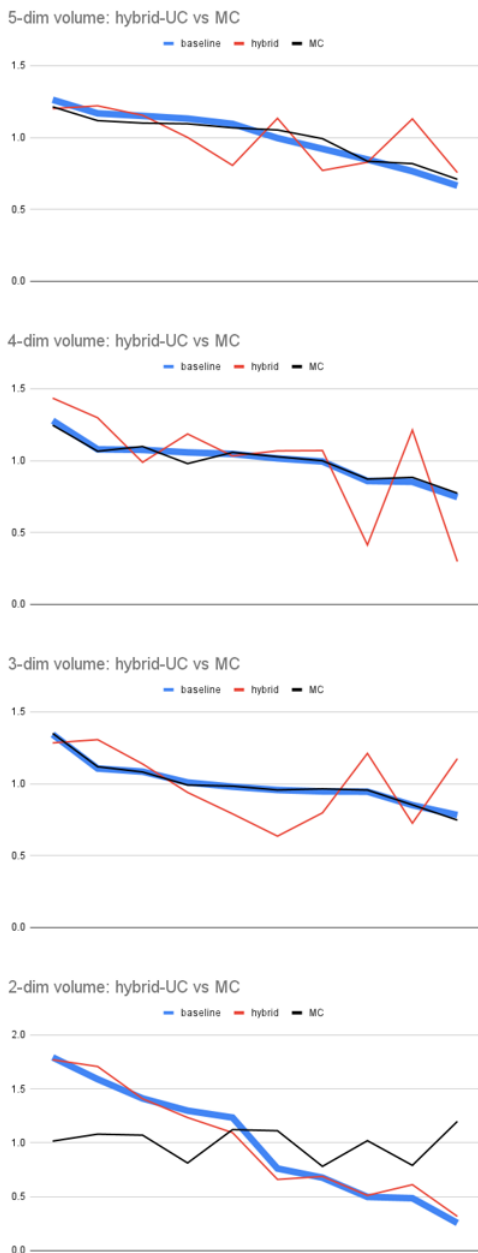


FIG. 9. Volume comparison for 5, 4, 3, and 2-dim test cases (top to bottom): relative volume among baseline (thick blue), hybrid-UC (red), and Monte Carlo (black).

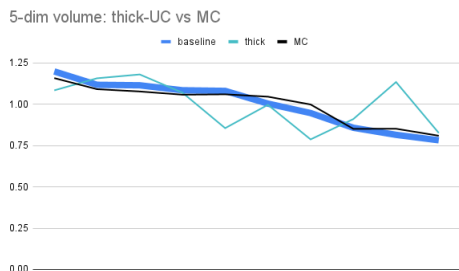


FIG. 10. Volume result for 5-dim test cases: relative volume among baseline (thick blue), thick-UC (cyan), and Monte Carlo (black).

as shown in figs 9 and 10.

Results above clearly show that UC generates more accurate volume result than EASAL. This proves that UC is a superior way of calculating configurational space volume for two-body distance constraint systems. Among variants of UC, hybrid method shows the best accuracy in volume calculation. This is mainly because its ability to greatly mitigate error in linearization mentioned in 5. In some extreme cases in lower dimension, regular or basis UC would wrongly deem all starting cubes as no intersection, even though there are feasible points in those cubes (such cubes are generated with feasible points sampled in run 0 by regular EASAL as centers), thus resulting in volume of 0 for some of the configurational spaces. Improved decomposition strategy, on the other hand, was able to fix those cases and finding intersections for those cubes. It is worth noting that all variants of UC deviates on volume result for certain configuration spaces. We speculate this is caused by those spaces being narrow in one (or more) of the dimensions, thus they are closer to lower-dimensional entities. This magnifies the error due to relatively coarse resolution we are using, and we expect users to analyze systems with such trait using finer resolution.

We picked hybrid-UC as method of our choice to compete against existing mainstream method, namely Monte Carlo. We also compared thick-UC with MC in 5-dim case. For higher dimensional input cases, UC provides volume results comparable to MC with a fraction of total sample count, as shown in sample count plots. For lower dimension (especially for 2-dim), MC’s drawback in sampling low dimensional region get exposed. Staying in the 6-dimensional space means it could not generate meaningful result, showcasing UC’s superiority on lower dimensional space volume calculation.

2. Efficiency Result

Fig 11 shows number of samples performed for each method totaled over 10 test cases for each dimensionality. From this we can clearly see that UC reaches such level of volume accuracy with way fewer samples than MC in higher dimensional test cases; in lower dimensional ones, MC fails to find enough test cases to meaningfully “sample” the region, thus UC (especially hybrid) shows its advantage.

Fig 12 shows time cost per point contributing to volume calculation for both UC variants and EASAL. Comparing them we can see that its superior volume calculation accuracy comes with a significant expense w.r.t. time, although the formal complexity analysis indicates no difference, i.e. linear time complexity in the output size for all methods (see III C).

Among UC variants, basis-UC handles each sample quicker when dimensionality gets lower. Due to its nature of stopping decomposition procedure on hyper-parallelepiped (rather than simplex) level, number of linear combination calls is significantly lowered, which is further augmented when R ’s dimensionality is low, $|E(G)|$ is large, hence decomposing hyper-parallelepiped into simplices takes significantly more time, which basis-UC completely skips. However, it also comes with lowest sample-per-point ratio, probably because of high



FIG. 11. Sample count for 5-, 4-, 3-, and 2-dim configuration spaces (top to bottom) using different methods: hybrid - red, regular - yellow, basis - green, thick - cyan, MC - black.

error (due to over-aggressive linearization) causing it to find intersections in other cubes, many of which are already found feasible.

As a direct optimization to regular-UC, hybrid-UC pays extra cost to fix linearization error. Their sample-per-point ratio is similar, demonstrating that extra samples of hybrid-UC did generate feasible cubes which were not found by regular-UC, instead of being wasted on already found ones. Results on time-per-point ratio show the trade-off between hybrid-UC being more accurate (while spending significantly more time to generate each sample point) and regular-UC being

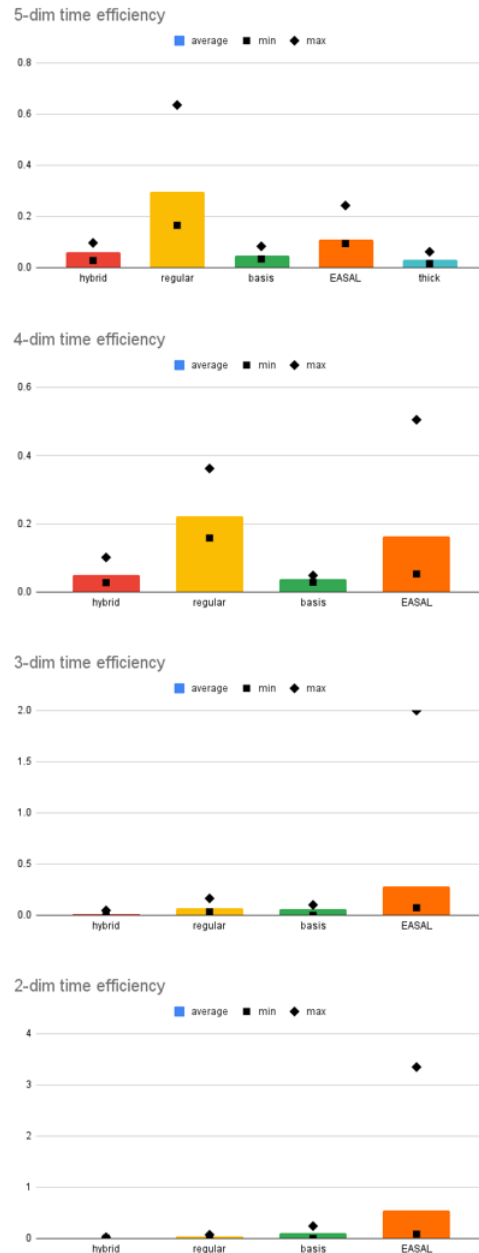


FIG. 12. Time efficiency results for 5-, 4-, 3-, and 2-dim configuration spaces (top to bottom): number of samples found per second that contributes to volume calculation using different methods: hybrid - red, regular - yellow, basis - green, thick - cyan. Higher means better.

faster, giving our potential users another parameter to customize based on their needs.

3. Coverage Result

As shown in fig 13, EASAL-UC variant of our choice (hybrid for all dimensionality and thick for 5-dim) shows significantly better coverage for the sampled region than regular EASAL, especially for higher dimensional configurational

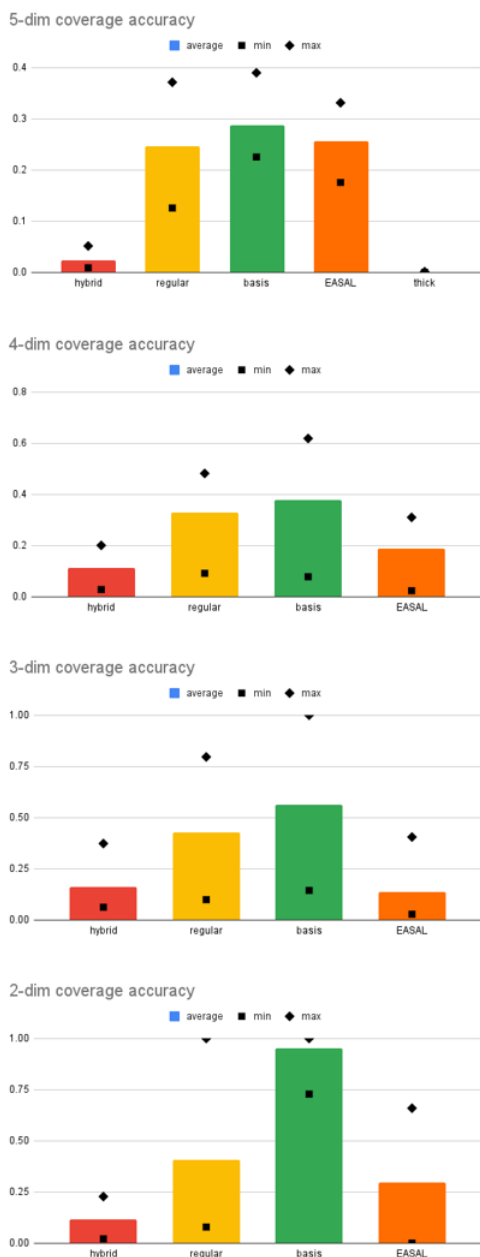


FIG. 13. Coverage missing ratio for 5-, 4-, 3-, and 2-dim configuration spaces (top to bottom) using different methods: hybrid - red, regular - yellow, basis - green, thick - cyan. Lower means better.

spaces which EASAL struggles on. It is specifically worth noting that thick-UC covers 99.9% on average, which is a huge improvement for regular EASAL⁴².

Fig 14 plots the number of sample points μ that lie in an γ -grid-hypercube against number of γ -hypercubes with μ sampled points. A more efficient method should have fewer points mapped to the same γ -cube, i.e. higher bars on the left side of the plot. As is seen in the plot, both hybrid-UC and EASAL show reasonably good result thanks to directly sampling the lower dimensional region with the highest bar on $\mu = 1$. On the contrary, MC peaks around $\mu = 10$ regardless of dimen-

sionality, illustrating its low efficiency in sampling especially for lower dimensional regions.

4. Asymmetry Difference

All 36 pairs of volume ratio between $A_i B_j$ and $A_j B_i$ are calculate using 3 different ways of volume calculation: hybrid-UC, EASAL, and Monte Carlo. Result is then ranked and compared with⁴⁴ using the DispLASA ranking method, as shown in fig 15.

Monte Carlo puts the top 3 results at the bottom, which is highly undesirable. Both UC and EASAL makes some improvement over MC, but there is still room for improvement.

V. FUTURE WORK

(1) Given the convex base space in Cayley coordinates, the randomized sampling for computing volumes of convex bodies given by^{62–66} could potentially be used to solve Problem 1 directly, thus bypassing Problem 2. However, to translate this to an accurate computation of the covering space poses a challenge: although the covering map is quite well behaved, this cannot be said about the pseudoinverses of its Jacobian or Hessian.

(2) The tradeoff between accuracy and efficiency both in volume computation and coverage is clearly demonstrated in the comparisons between EASAL-UC and the comparator methods that rely on sampling entirely in Cayley coordinates. Hybridizing these methods in a manner appropriate to requirements of specific applications is indicated.

(3) Optimization in EASAL-UC implementation is expected to reduce numerical errors and improve performance on larger $|S|$.

(4) Although the comparator methods have been recently compared with prevailing methods in⁴⁴, a direct comparison of EASAL-UC with prevailing methods is indicated.

(5) It remains to test EASAL-UC for configurational entropy, free energy, binding affinity, and hot-spot residue computations on well known benchmark datasets for Lennard-Jones clusters, ligand docking and computational alanine scanning^{68–70}. The longer term goal is to demonstrate use of EASAL-UC’s efficient computation of the above quantities to make concrete progress on specific, poorly understood, soft matter assembly systems.

¹M. Casiulis and S. Martiniani, “When you can’t count, sample! computable entropies beyond equilibrium from basin volumes,” *Papers in Physics* **15** (2022), 10.4279/pip.150001.

²O. B. Eriçok and J. K. Mason, “Quotient maps and configuration spaces of hard disks,” *Granular Matter* **24**, 1–15 (2022).

³O. B. Eriçok, K. Ganesan, and J. K. Mason, “Configuration spaces of hard spheres,” *Physical Review E* **104**, 055304 (2021).

⁴M. Hütter, “Configurational entropy of a finite number of dumbbells close to a wall,” *The European Physical Journal E* **45**, 1–19 (2022).

⁵L. Chan, G. M. Morris, and G. R. Hutchison, “Understanding conformational entropy in small molecules,” *Journal of Chemical Theory and Computation* **17**, 2099–2106 (2021).

⁶M. Karplus and J. N. Kushick, “Method for estimating the configurational entropy of macromolecules,” *Macromolecules* **14**, 325–332 (1981).

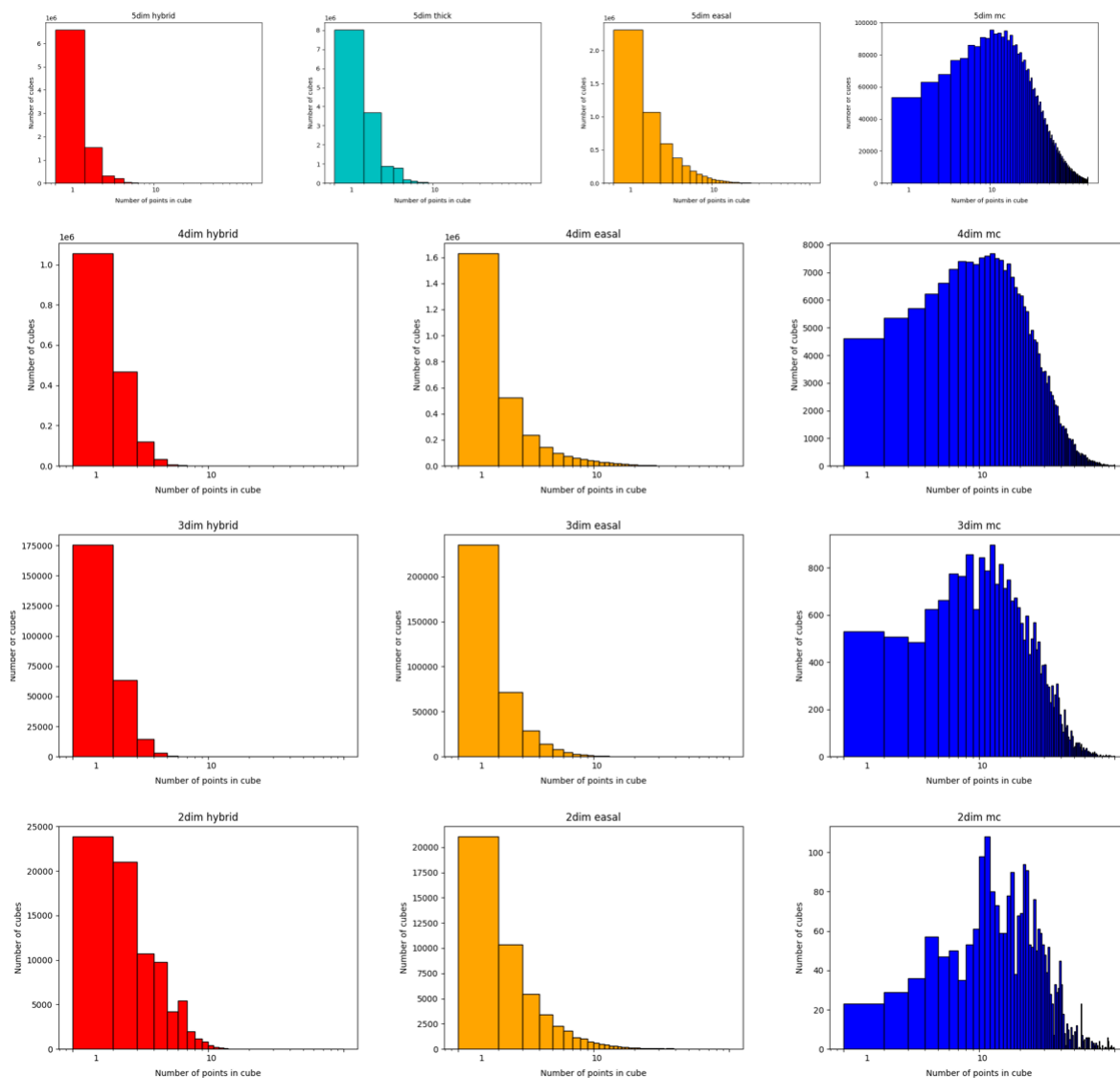


FIG. 14. Coverage efficiency for 5, 4, 3, and 2-dim test cases (top to bottom) using different methods: hybrid - red, thick - cyan, EASAL - orange, MC - blue. In each subplot, horizontal axis shows the number (or fraction) of sample points v that lie in γ -cubes and vertical axis shows the number of γ -cubes having v mapped points in them. Better method should have higher blocks towards left side of plot.

- ⁷N. Go, T. Noguti, and T. Nishikawa, "Dynamics of a small globular protein in terms of low-frequency vibrational modes," *Biophysics* **80**, 3696–3700 (1983).
- ⁸R. M. Levy, M. Karplus, J. Kushick, and D. Perahia, "Evaluation of the configurational entropy for proteins: Application to molecular dynamics simulations of an α -helix," *Macromolecules* **17**, 1370–1374 (1984).
- ⁹M. Karplus, T. Ichiye, and B. M. Pettitt, "Configurational entropy of native proteins," *Biophysical Journal* **52**, 1083–1085 (1987).
- ¹⁰M. H. Hao and H. A. Scheraga, "Monte carlo simulation of a first-order transition for protein folding," *Journal of Physical Chemistry* **98**, 4940–4948 (1994).
- ¹¹F. Fogolari, A. Corazza, S. Fortuna, M. A. Soler, B. V. Schouwen, G. Brancolini, S. Corni, G. Melacini, and G. Esposito, "Distance-based configurational entropy of proteins from molecular dynamics simulations," *PLoS ONE* **10**, 1–26 (2015).
- ¹²K. K. Frederick, M. S. Marlow, K. G. Valentine, and A. J. Wand, "Conformational entropy in molecular recognition by proteins," *Nature* **448**, 325–329 (2007).
- ¹³A. M. Ruvinsky, "Role of binding entropy in the refinement of protein–ligand docking predictions: Analysis based on the use of 11 scoring functions," *Journal of Computational Chemistry* **28**, 1364–1372 (2007).
- ¹⁴M. A. Lill, "Efficient incorporation of protein flexibility and dynamics into molecular docking simulations," *Biochemistry* **50**, 6157–6169 (2011).
- ¹⁵C. E. A. Chang, W. Chen, and M. K. Gilson, "Ligand configurational entropy and protein binding," *Proceedings of the National Academy of Sciences of the United States of America* **104**, 1534–1539 (2007).
- ¹⁶Z. Sun, Y. N. Yan, M. Yang, and J. Z. Zhang, "Interaction entropy for protein-protein binding," *Journal of Chemical Physics* **146** (2017), 10.1063/1.4978893.
- ¹⁷L. Qiu, Y. Yan, Z. Sun, J. Song, and J. Z. Zhang, "Interaction entropy for computational alanine scanning in protein–protein binding," *Wiley Interdisciplinary Reviews: Computational Molecular Science* **8** (2018), 10.1002/wcms.1342.
- ¹⁸C. Gao, M. S. Park, and H. A. Stern, "Accounting for ligand conformational restriction in calculations of protein–ligand binding affinities," *Biophysical Journal* **98** (2010), 10.1016/j.bpj.2009.11.018.

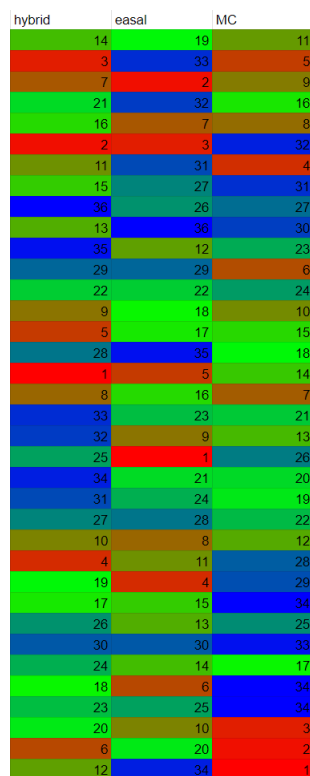


FIG. 15. Volume ratio between $A_i B_j - A_j B_i$ pairs using different methods: hybrid-UC - left, EASAL - mid, and Monte Carlo - right. Better method will have ranking with red entries at the top and blue entries at the bottom.

- ¹⁹K. W. Harpole and K. A. Sharp, "Calculation of configurational entropy with a boltzmann-quasiharmonic model: The origin of high-affinity protein-ligand binding," *Journal of Physical Chemistry B* **115**, 9461–9472 (2011).
- ²⁰L. Duan, X. Liu, and J. Z. Zhang, "Interaction entropy: A new paradigm for highly efficient and reliable computation of protein-ligand binding free energy," *Journal of the American Chemical Society* **138**, 5722–5728 (2016).
- ²¹M. L. Verteramo, O. Stenström, M. M. Ignjatović, O. Caldararu, M. A. Olsson, F. Manzoni, H. Leffler, E. Oksanen, D. T. Logan, U. J. Nilsson, U. Ryde, and M. Akke, "Interplay between conformational entropy and solvation entropy in protein-ligand binding," *Journal of the American Chemical Society* **141**, 2012–2026 (2019).
- ²²D. A. Case, T. E. Cheatham, T. Darden, H. Gohlke, R. Luo, K. M. Merz, A. Onufriev, C. Simmerling, B. Wang, and R. J. Woods, "The amber biomolecular simulation programs," *Journal of Computational Chemistry* **26**, 1668–1688 (2005).
- ²³S. Chelvaraja and H. Meirovitch, "Simulation method for calculating the entropy and free energy of peptides and proteins," *Proceedings of the National Academy of Sciences* **101**, 9241–9246 (2004).
- ²⁴C. D. Schwieters and G. M. Clore, "Internal coordinates for molecular dynamics and minimization in structure determination and refinement," *Journal of magnetic resonance (San Diego, Calif. : 1997)* **152**, 288–302 (2001).
- ²⁵G. A. Tribello and P. Gasparotto, "Using dimensionality reduction to analyze protein trajectories," *Frontiers in Molecular Biosciences* **6** (2019), 10.3389/fmolb.2019.00046.
- ²⁶P. Pulay, G. Fogarasi, F. Pang, and J. E. Boggs, "Systematic ab initio gradient calculation of molecular geometries, force constants, and dipole moment derivatives," *Journal of the American Chemical Society* **101**, 2550–2560 (1979).
- ²⁷G. Fogarasi, X. Zhou, P. W. Taylor, and P. Pulay, "The calculation of ab initio molecular geometries: Efficient optimization by natural internal coordinates and empirical correction by offset forces," *Journal of the American Chemical Society* **114**, 8191–8201 (1992).
- ²⁸P. Pulay and G. Fogarasi, "Geometry optimization in redundant internal coordinates," *The Journal of Chemical Physics* **96**, 2856–2860 (1992).
- ²⁹C. Peng, P. Y. Ayala, H. B. Schlegel, and M. J. Frisch, "Using redundant internal coordinates to optimize equilibrium geometries and transition states," *Journal of Computational Chemistry* **17**, 49–56 (1996).
- ³⁰J. Baker, A. Kessi, and B. Delley, "The generation and use of delocalized internal coordinates in geometry optimization," *The Journal of Chemical Physics* **105**, 192–212 (1996).
- ³¹J. Baker, D. Kinghorn, and P. Pulay, "Geometry optimization in delocalized internal coordinates: An efficient quadratically scaling algorithm for large molecules," *Journal of Chemical Physics* **110**, 4986–4991 (1999).
- ³²V. V. Rybkin, U. Ekström, and T. Helgaker, "Internal-to-cartesian back transformation of molecular geometry steps using high-order geometric derivatives," *Journal of Computational Chemistry* **34**, 1842–1849 (2013).
- ³³K. Oenen, D. F. Dinu, and K. R. Liedl, "Determining internal coordinate sets for optimal representation of molecular vibration," *The Journal of Chemical Physics* **160**, 014104 (2024), https://pubs.aip.org/aip/jcp/article-pdf/doi/10.1063/5.0180657/18287665/014104_1_5.0180657.pdf.
- ³⁴L. P. Wang and C. Song, "Geometry optimization made simple with translation and rotation coordinates," *Journal of Chemical Physics* **144**, 214108 (2016).
- ³⁵M. Bayati, M. Leeser, and J. P. Bardhan, "High-performance transformation of protein structure representation from internal to cartesian coordinates," *Journal of Computational Chemistry* **41**, 2104–2114 (2020).
- ³⁶J. Li, O. Zhang, S. Lee, A. Namini, Z. H. Liu, J. M. Teixeira, J. D. Forman-Kay, and T. Head-Gordon, "Learning correlations between internal coordinates to improve 3d cartesian coordinates for proteins," *Journal of Chemical Theory and Computation* **19**, 4689–4700 (2023).
- ³⁷J. Demmel, "Nearest defective matrices and the geometry of ill-conditioning," *Reliable Numerical Computation*, 35–56 (1990).
- ³⁸H.-X. Zhou and M. K. Gilson, "Theory of free energy and entropy in noncovalent binding," *Chemical Reviews* **109**, 4092–4107 (2009), pMID: 19588959.
- ³⁹D. J. Wales and T. V. Bogdan, "Potential energy and free energy landscapes," *The Journal of Physical Chemistry B* **110**, 20765–20776 (2006), pMID: 17048885.
- ⁴⁰G. Bussi and D. Branduardi, "Free-energy calculations with metadynamics: Theory and practice," in *Reviews in Computational Chemistry Volume 28* (John Wiley & Sons, Ltd, 2015) Chap. 1, pp. 1–49, <https://onlinelibrary.wiley.com/doi/pdf/10.1002/9781118889886.ch1>.
- ⁴¹A. Ozkan, R. Prabhu, T. Baker, J. Pence, J. Peters, and M. Sitharam, "Algorithm 990: Efficient atlasing and search of configuration spaces of point-sets constrained by distance intervals," *ACM Transactions on Mathematical Software* **44** (2018), 10.1145/3204472.
- ⁴²R. Prabhu, M. Sitharam, A. Ozkan, and R. Wu, "Atlasing of assembly landscapes using distance geometry and graph rigidity," *Journal of Chemical Information and Modeling* **60**, 4924–4957 (2020).
- ⁴³J. Youngquist, M. Sitharam, and J. Peters, "A slice-traversal algorithm for very large mapped volumetric models," *Computer-Aided Design* **141**, 103102 (2021).
- ⁴⁴A. Ozkan, M. Sitharam, J. C. Flores-Canales, R. Prabhu, and M. Kurnikova, "Baseline comparisons of complementary sampling methods for assembly driven by short-ranged pair potentials toward fast and flexible hybridization," *Journal of Chemical Theory and Computation* **17**, 1967–1987 (2021).
- ⁴⁵J. E. Graver, B. Servatius, and H. Servatius, *Combinatorial rigidity* (American Mathematical Soc., 1993).
- ⁴⁶M. Sitharam, A. S. John, and J. Sidman, *Handbook of geometric constraint systems principles* (Chapman and Hall/CRC, 2018).
- ⁴⁷S. Seo and W. Shinoda, "Molecular dynamics simulations," in *Reference Module in Chemistry, Molecular Sciences and Chemical Engineering* (Elsevier, 2018).
- ⁴⁸M. Sitharam and H. Gao, "Characterizing graphs with convex and connected cayley configuration spaces," *Discrete and Computational Geometry* **43**, 594–625 (2010).
- ⁴⁹M. Sitharam and M. Wang, "How the beast really moves: Cayley analysis of mechanism realization spaces using caymos," *Computer-Aided Design* **46**, 205–210 (2014), 2013 SIAM Conference on Geometric and Physical Modeling.

- ⁵⁰M. Wang and M. Sitharam, “Algorithm 951: Cayley analysis of mechanism configuration spaces using caymos: Software functionalities and architecture,” *ACM Trans. Math. Softw.* **41**, 27:1–27:8 (2015).
- ⁵¹M. Sitharam, M. Wang, and H. Gao, “Cayley configuration spaces of 2d mechanisms, part i: extreme points, continuous motion paths and minimal representations,” (2011).
- ⁵²M. Sitharam, M. Wang, and H. Gao, “Cayley configuration spaces of 1-dof tree-decomposable linkages, part ii: Combinatorial characterization of complexity,” (2011).
- ⁵³I. J. Schoenberg, “Metric spaces and positive definite functions,” *Transactions of the American Mathematical Society* **44**, 522–536 (1938).
- ⁵⁴K. Ball, “Isometric embedding in lp-spaces,” *European Journal of Combinatorics* **11**, 305–311 (1990).
- ⁵⁵M. Sitharam and J. Willoughby, “On flattenability of graphs,” *Proceedings of the ADG* (2015).
- ⁵⁶M. Belk and R. Connelly, “Realizability of graphs,” *Discrete and Computational Geometry* **37**, 125–137 (2007).
- ⁵⁷M. Belk, “Realizability of graphs in three dimensions,” *Discrete & Computational Geometry* **37**, 139–162 (2007).
- ⁵⁸T. Baker, M. Sitharam, M. Wang, and J. Willoughby, “Optimal decomposition and recombination of isostatic geometric constraint systems for designing layered materials,” *Computer Aided Geometric Design* **40** (2015), 10.1016/j.cagd.2015.07.001.
- ⁵⁹S. Hikiri, T. Yoshidome, and M. Ikeguchi, “Computational methods for configurational entropy using internal and cartesian coordinates,” *Journal of Chemical Theory and Computation* **12**, 5990–6000 (2016).
- ⁶⁰G. Gyimesi, P. Závodszy, and A. Szilágyi, “Calculation of configurational entropy differences from conformational ensembles using gaussian mixtures,” *Journal of Chemical Theory and Computation* **13**, 29–41 (2017).
- ⁶¹A. Ozkan and M. Sitharam, “Best of both worlds: Uniform sampling in cartesian and cayley molecular assembly configuration space,” , 7–10 (2014).
- ⁶²M. Dyer, A. Frieze, and R. Kannan, “A random polynomial-time algorithm for approximating the volume of convex bodies,” *J. ACM* **38**, 1–17 (1991).
- ⁶³D. Applegate and R. Kannan, “Sampling and integration of near log-concave functions,” in *Proceedings of the Twenty-Third Annual ACM Symposium on Theory of Computing, STOC '91* (Association for Computing Machinery, New York, NY, USA, 1991) p. 156–163.
- ⁶⁴R. Kannan, L. Lovász, and M. Simonovits, “Random walks and an $o^*(n^5)$ volume algorithm for convex bodies,” *Random Structures & Algorithms* **11**, 1–50 (1997).
- ⁶⁵L. Lovász and S. Vempala, “Simulated annealing in convex bodies and an $o^*(n^4)$ volume algorithm,” *Journal of Computer and System Sciences* **72**, 392–417 (2006), jCSS FOCS 2003 Special Issue.
- ⁶⁶C. Ge and F. Ma, “A fast and practical method to estimate volumes of convex polytopes,” in *Frontiers in Algorithmics - 9th International Workshop, FAW 2015, Guilin, China, July 3-5, 2015, Proceedings*, Lecture Notes in Computer Science, Vol. 9130, edited by J. Wang and C. Yap (Springer, 2015) pp. 52–65.
- ⁶⁷M. Sitharam and Y. Zhang, “Best of two worlds: Cartesian sampling and volume computation for high dimensional configuration spaces using cayley coordinates,” *The 30th Annual Fall Workshop on Computational Geometry* (2022).
- ⁶⁸L. Trombach, R. S. Hoy, D. J. Wales, and P. Schwerdtfeger, “From sticky-hard-sphere to lennard-jones-type clusters,” *Phys. Rev. E* **97**, 043309 (2018).
- ⁶⁹J. Jankauskaitė, B. Jiménez-García, J. Dapkūnas, J. Fernández-Recio, and I. H. Moal, “SKEMPI 2.0: an updated benchmark of changes in protein–protein binding energy, kinetics and thermodynamics upon mutation,” *Bioinformatics* **35**, 462–469 (2018).
- ⁷⁰P. Agrawal, H. Singh, H. Srivastava, S. Singh, G. Kishor, and G. Raghava, “Benchmarking of different molecular docking methods for protein-peptide docking,” *BMC Bioinformatics* **19** (2019), 10.1186/s12859-018-2449-y.
- ⁷¹R. Wu, A. Ozkan, A. Bennett, M. Agbandje-Mckenna, and M. Sitharam, “Robustness measure for an adeno-associated viral shell self-assembly is accurately predicted by configuration space atlas using easal,” 2012 ACM Conference on Bioinformatics, Computational Biology and Biomedicine, BCB 2012 , 690–695 (2012).
- ⁷²R. Wu, R. Prabhu, A. Ozkan, and M. Sitharam, “Rapid prediction of crucial hotspot interactions for icosahedral viral capsid self-assembly by energy landscape atlas validated by mutagenesis,” *PLoS Computational Biology* **16** (2020), 10.1371/journal.pcbi.1008357.
- ⁷³M. Wang and M. Sitharam, “Combinatorial rigidity and independence of generalized pinned subspace-incidence constraint systems,” *Proceedings of the ADG* (2015).
- ⁷⁴S. Hikiri, T. Yoshidome, and M. Ikeguchi, “Computational methods for configurational entropy using internal and cartesian coordinates,” *Journal of Chemical Theory and Computation* **12**, 5990–6000 (2016).
- ⁷⁵F. Fogolari, A. Corazza, S. Fortuna, M. A. Soler, B. V. Schouwen, G. Brancolini, S. Corni, G. Melacini, and G. Esposito, “Distance-based configurational entropy of proteins from molecular dynamics simulations,” *PLoS ONE* **10**, 1–26 (2015).
- ⁷⁶M. Holmes-Cerfon, S. J. Gortler, and M. P. Brenner, “A geometrical approach to computing free-energy landscapes from short-ranged potentials,” *Proceedings of the National Academy of Sciences of the United States of America* **110** (2013), 10.1073/pnas.1211720110.
- ⁷⁷A. R. Dinner, E. H. Thiede, B. V. Kotev, and J. Weare, “Stratification as a general variance reduction method for markov chain monte carlo,” *SIAM-ASA Journal on Uncertainty Quantification* **8**, 1139–1188 (2017).
- ⁷⁸G. Gyimesi, P. Závodszy, and A. Szilágyi, “Calculation of configurational entropy differences from conformational ensembles using gaussian mixtures,” *Journal of Chemical Theory and Computation* **13**, 29–41 (2017).
- ⁷⁹M. Goethe, J. Gleixner, I. Fita, and J. M. Rubi, “Prediction of protein configurational entropy (popcoen),” *Journal of Chemical Theory and Computation* **14**, 1811–1819 (2018).
- ⁸⁰J. Jankauskaite, B. Jiménez-García, J. Dapkunas, J. Fernández-Recio, and I. H. Moal, “Skempi 2.0: An updated benchmark of changes in protein-protein binding energy, kinetics and thermodynamics upon mutation,” *Bioinformatics* **35**, 462–469 (2019).
- ⁸¹P. Richet, “Viscosity and configurational entropy of silicate melts,” *Geochimica et Cosmochimica Acta* **48**, 471–483 (1984).
- ⁸²S. V. Krivovichev, “Structural complexity and configurational entropy of crystals,” *urn:issn:2052-5206* **72**, 274–276 (2016).
- ⁸³J. D. Sartor and E. I. Corwin, “Direct measurement of force configurational entropy in jamming,” *Physical Review E* **101** (2020), 10.1103/PHYSREVE.101.050902.
- ⁸⁴O. K. Vorov, D. R. Livesay, and D. J. Jacobs, “Conformational entropy of an ideal cross-linking polymer chain,” *Entropy* 2008, Vol. 10, Pages 285–308 **10**, 285–308 (2008).
- ⁸⁵B. J. Killian, J. Y. Kravitz, and M. K. Gilson, “Extraction of configurational entropy from molecular simulations via an expansion approximation,” *Journal of Chemical Physics* **127**, 24107 (2007).
- ⁸⁶E. P. George, D. Raabe, and R. O. Ritchie, “High-entropy alloys,” *Nature Reviews Materials* 2019 4:8 **4**, 515–534 (2019).
- ⁸⁷J. Li, O. Zhang, S. Lee, A. Namini, Z. H. Liu, J. M. Teixeira, J. D. Forman-Kay, and T. Head-Gordon, “Learning correlations between internal coordinates to improve 3d cartesian coordinates for proteins,” *Journal of Chemical Theory and Computation* **19**, 4689–4700 (2022).
- ⁸⁸J. M. Teixeira, Z. H. Liu, A. Namini, J. Li, R. M. Vernon, M. Krzeminski, A. A. Shamandy, O. Zhang, M. Haghighatdari, L. Yu, T. Head-Gordon, and J. D. Forman-Kay, “Idpconformergenerator: A flexible software suite for sampling the conformational space of disordered protein states,” *Journal of Physical Chemistry A* **126**, 5985–6003 (2022).